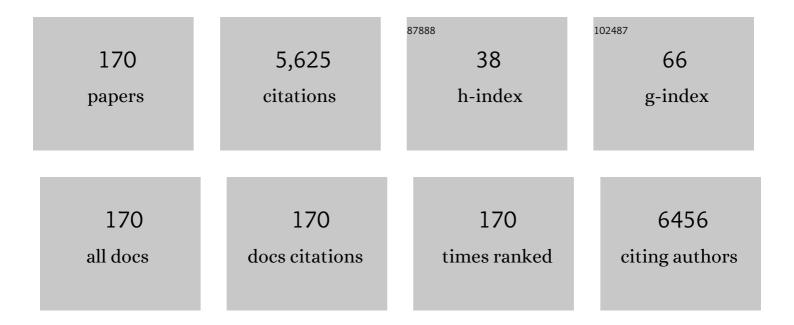
List of Publications by Year in descending order

Source: https://exaly.com/author-pdf/6908878/publications.pdf Version: 2024-02-01



LINC-POL

#	Article	IF	CITATIONS
1	Hierarchical V2O5 microspheres: A pseudocapacitive cathode material for enhanced sodium ion storage. Journal of Alloys and Compounds, 2022, 895, 162617.	5.5	3
2	Influence of the charge compensation effect on the metal–insulator transition of Mg-W co-doped VO2. Applied Surface Science, 2022, 579, 151990.	6.1	18
3	Optimizing the Na metal/solid electrolyte interface through a grain boundary design. Journal of Materials Chemistry A, 2022, 10, 5280-5286.	10.3	18
4	Design of highly reflective film for smart radiation device. Vibroengineering PROCEDIA, 2022, 40, 132-138.	0.5	4
5	Prussianâ€blue materials: Revealing new opportunities for rechargeable batteries. InformaÄnÃ-Materiály, 2022, 4, .	17.3	73
6	W-VO ₂ /Cs _{0.32} WO ₃ Composite Flexible Films: Promoted Metal–Insulator Transition and Enhanced Near-Infrared Shielding. ACS Applied Energy Materials, 2022, 5, 3064-3071.	5.1	7
7	Solidâ€State Na Metal Batteries with Superior Cycling Stability Enabled by Ferroelectric Enhanced Na/Na ₃ Zr ₂ Si ₂ PO ₁₂ Interface. Small, 2022, 18, e2200716.	10.0	24
8	Thermochromic VO2 based sandwich structure Ag/Al2O3/VO2 with low solar absorption and tunable emittance for spacecraft. Journal of Applied Physics, 2022, 131, .	2.5	7
9	0D/1D/2D architectural Co@C/MXene composite for boosting microwave attenuation performance in 2–18ÂGHz. Carbon, 2022, 193, 182-194.	10.3	108
10	Reversible multielectron redox in NASICON cathode with high energy density for low-temperature sodium-ion batteries. Energy Storage Materials, 2022, 49, 291-298.	18.0	43
11	Dualâ€Function of Cationâ€Doping to Activate Cationic and Anionic Redox in a Mnâ€Based Sodiumâ€Layered Oxide Cathode. Small, 2022, 18, e2200289.	10.0	10
12	VO2(M)@SnO2 core–shell nanoparticles: Improved chemical stability and thermochromic property rendered by SnO2 shell. Applied Surface Science, 2022, 598, 153741.	6.1	12
13	Minimizing the interfacial resistance for a solid-state lithium battery running at room temperature. Chemical Engineering Journal, 2022, 448, 137740.	12.7	27
14	Optimizing phase transition temperature and visible transmittance of VO2 films driven by synergistic effect of La-Mo co-doping. Applied Surface Science, 2022, 600, 154074.	6.1	7
15	Correlating the gradient nitrogen doping and electromagnetic wave absorption of graphene at gigahertz. Journal of Alloys and Compounds, 2021, 854, 157113.	5.5	20
16	Dielectric relaxation and conduction behaviors of Aurivillius Na0.5Bi4.5Ti4O15 ceramics with Na doping. Rare Metals, 2021, 40, 1247-1254.	7.1	5
17	Hole Dopants Disentangling Peierls–Mott Relevance States of VO ₂ by First-Principles Calculation. Journal of Physical Chemistry C, 2021, 125, 5816-5823.	3.1	13
18	Phase Manipulating toward Molybdenum Disulfide for Optimizing Electromagnetic Wave Absorbing in Gigahertz. Advanced Functional Materials, 2021, 31, 2011229.	14.9	141

#	Article	IF	CITATIONS
19	Importance of Crystallographic Sites on Sodium-Ion Extraction from NASICON-Structured Cathodes for Sodium-Ion Batteries. ACS Applied Materials & amp; Interfaces, 2021, 13, 14312-14320.	8.0	35
20	Electric field driven abnormal increase in conductivity of tungsten-doped VO2 nanofilms. Thin Solid Films, 2021, 725, 138643.	1.8	15
21	Synthesis and thermoelectric performance of Ni0.3Co3.7Sb12 skutterudite filled with electronegative guest Se. Ceramics International, 2021, 47, 17753-17759.	4.8	6
22	Size-Controllable M-Phase VO ₂ Nanocrystals for Flexible Thermochromic Energy-Saving Windows. ACS Applied Nano Materials, 2021, 4, 6778-6785.	5.0	24
23	Dumbbell-Like Fe ₃ O ₄ @N-Doped Carbon@2H/1T-MoS ₂ with Tailored Magnetic and Dielectric Loss for Efficient Microwave Absorbing. ACS Applied Materials & Interfaces, 2021, 13, 47061-47071.	8.0	62
24	Grain Boundary Design of Solid Electrolyte Actualizing Stable All‣olid‣tate Sodium Batteries. Small, 2021, 17, e2103819.	10.0	29
25	Experimental and theoretical investigation of Na4MnAl(PO4)3 cathode material for sodium-ion batteries. Chemical Engineering Journal, 2021, 425, 130680.	12.7	29
26	Utilization of the V5+/V4 + Redox Reaction in Nasicon-Structured Cathode Materials for Sodium-Ion Batteries. ECS Meeting Abstracts, 2021, MA2021-02, 1695-1695.	0.0	0
27	Oxygen vacancy boosted the electrochemistry performance of Ti4+ doped Nb2O5 toward lithium ion battery. Applied Surface Science, 2020, 499, 143905.	6.1	38
28	Dielectric behaviors and electrical properties of Gd-doped Aurivillius KBi4Ti4O15 ceramics. Journal of Materials Science: Materials in Electronics, 2020, 31, 14674-14680.	2.2	2
29	Triggering the Reversible Reaction of V ³⁺ /V ⁴⁺ /V ⁵⁺ in Na ₃ V ₂ (PO ₄) ₃ by Cr ³⁺ Substitution. ACS Applied Materials & Interfaces, 2020, 12, 50315-50323.	8.0	47
30	Key Experiments and Thermodynamic Description of the Co-Nb-Ni System. Metallurgical and Materials Transactions A: Physical Metallurgy and Materials Science, 2020, 51, 5892-5911.	2.2	11
31	Sn–W Co-doping Improves Thermochromic Performance of VO ₂ Films for Smart Windows. ACS Applied Energy Materials, 2020, 3, 9972-9979.	5.1	30
32	Microstructural control of Co3O4 nanoboxes for enhanced oxygen evolution in alkaline media. Journal of Alloys and Compounds, 2020, 835, 155290.	5.5	7
33	Dielectric relaxation and electrical properties of Na0.5Bi4La0.5Ti4O15 electroceramics. Journal of Electroceramics, 2020, 44, 147-153.	2.0	1
34	Sn dopants improve the visible transmittance of VO2 films achieving excellent thermochromic performance for smart window. Solar Energy Materials and Solar Cells, 2020, 209, 110443.	6.2	50
35	Ultrathin MoS ₂ Nanosheets Encapsulated in Hollow Carbon Spheres: A Case of a Dielectric Absorber with Optimized Impedance for Efficient Microwave Absorption. ACS Applied Materials & Interfaces, 2020, 12, 20785-20796.	8.0	120
36	First-principle calculation of electronic and optical properties of VO2 by GGA-1/2 quasiparticle approximation. Journal of Applied Physics, 2020, 128, .	2.5	6

#	Article	IF	CITATIONS
37	Surface modification-assisted solvent annealing to prepare high quality M-phase VO2 nanocrystals for flexible thermochromic films. Solar Energy Materials and Solar Cells, 2019, 200, 110031.	6.2	18
38	Convenient Synthesis of WS ₂ –MoS ₂ Heterostructures with Enhanced Photocatalytic Performance. Journal of Physical Chemistry C, 2019, 123, 27363-27368.	3.1	15
39	W Doping and Voltage Driven Metal–Insulator Transition in VO ₂ Nano-Films for Smart Switching Devices. ACS Applied Nano Materials, 2019, 2, 6738-6746.	5.0	36
40	Thermodynamic modeling of elastic mismatch strain energy on epitaxial growth of GaInN thin films. Journal of Alloys and Compounds, 2019, 798, 112-118.	5.5	1
41	Vanadium-Substituted Formation of Anatase (V, Ti)O ₂ : Enhanced Electrochemical Performance for Lithium Ion Batteries. ACS Applied Energy Materials, 2019, 2, 598-606.	5.1	4
42	Layer by layer 2D MoS2/rGO hybrids: An optimized microwave absorber for high-efficient microwave absorption. Applied Surface Science, 2019, 470, 899-907.	6.1	62
43	Biopolymer nanofiber/reduced graphene oxide aerogels for tunable and broadband high-performance microwave absorption. Composites Part B: Engineering, 2019, 161, 1-9.	12.0	57
44	VO2 (A)/graphene nanostructure: Stand up to Na ion intercalation/deintercalation for enhanced electrochemical performance as a Na-ion battery cathode. Electrochimica Acta, 2019, 293, 97-104.	5.2	20
45	One-step fabrication of N-doped CNTs encapsulating M nanoparticles (M = Fe, Co, Ni) for efficient microwave absorption. Applied Surface Science, 2018, 447, 244-253.	6.1	115
46	Enhanced microwave absorption properties of Co-doped SiC at elevated temperature. Applied Surface Science, 2018, 445, 383-390.	6.1	46
47	The synthesis of FeCoS ₂ and an insight into its physicochemical performance. CrystEngComm, 2018, 20, 2175-2182.	2.6	17
48	Chemical reduction dependent dielectric properties and dielectric loss mechanism of reduced graphene oxide. Carbon, 2018, 127, 209-217.	10.3	268
49	Porous layer assembled hierarchical Co3O4 as anode materials for lithium-ion batteries. Journal of Materials Science, 2018, 53, 1356-1364.	3.7	18
50	Confining ferric oxides in porous carbon for efficient lithium storage. Electrochimica Acta, 2018, 292, 879-886.	5.2	14
51	Temperature dependent conductivity of Bi4Ti3O12 ceramics induced by Sr dopants. Journal of Advanced Ceramics, 2018, 7, 256-265.	17.4	16
52	Neat Design for the Structure of Electrode To Optimize the Lithium-Ion Battery Performance. ACS Applied Materials & Interfaces, 2018, 10, 27106-27115.	8.0	40
53	Graphene boosted pseudocapacitive lithium storage: A case of G-Fe2O3. Electrochimica Acta, 2018, 282, 955-963.	5.2	29
54	Hydrothermal One-Step Synthesis of Highly Dispersed M-Phase VO ₂ Nanocrystals and Application to Flexible Thermochromic Film. ACS Applied Materials & Interfaces, 2018, 10, 28627-28634.	8.0	56

#	Article	IF	CITATIONS
55	Microstructural Evolution in High-Strain-Rate Deformation of Ti-5Al-5Mo-5V-1Cr-1Fe Alloy. Materials, 2018, 11, 839.	2.9	1
56	Graphene oxide modified nano-sized BaTiO3 as photocatalyst. Ceramics International, 2018, 44, 15929-15934.	4.8	27
57	Design of hierarchical CuS/graphene architectures with enhanced lithium storage capability. Applied Surface Science, 2017, 403, 1-8.	6.1	57
58	Synthesis of NiO Nano Octahedron Aggregates as High-Performance Anode Materials for Lithium Ion Batteries. Electrochimica Acta, 2017, 231, 272-278.	5.2	81
59	Rational construction the composite of graphene and hierarchical structure assembled by Fe 2 O 3 nanosheets for lithium storage. Electrochimica Acta, 2017, 243, 18-25.	5.2	45
60	Enhanced composites of V2O5 nanowires decorating on graphene layers as ideal cathode materials for lithium-ion batteries. Journal of Alloys and Compounds, 2017, 695, 2974-2980.	5.5	26
61	The synthesis of hierarchical nanostructured MoS 2 /Graphene composites with enhanced visible-light photo-degradation property. Applied Surface Science, 2017, 412, 207-213.	6.1	68
62	The effect of artificial stress on Er 3+ doped perovskite lead-free piezoceramics. Journal of Alloys and Compounds, 2017, 709, 724-728.	5.5	10
63	Dielectric relaxation and electrical properties of Sm 0.5 Bi 4.5 Ti 3 FeO 15 ceramics. Journal of Alloys and Compounds, 2017, 709, 686-691.	5.5	14
64	Symmetric Confined Growth of Superstructured Vanadium Dioxide Nanonet with a Regular Geometrical Pattern by a Solution Approach. Crystal Growth and Design, 2017, 17, 5838-5844.	3.0	17
65	The effect of the phase structure on physicochemical properties of TMO materials: a case of spinel to bunsenite. CrystEngComm, 2017, 19, 5809-5814.	2.6	15
66	The synthesis of ultra-long cobalt chains and its outstanding catalytic performance on the thermal decomposition of ammonium perchlorate. Materials Chemistry and Physics, 2017, 201, 235-240.	4.0	10
67	Evolution of Structural and Electrical Properties of Oxygen-Deficient VO ₂ under Low Temperature Heating Process. ACS Applied Materials & Interfaces, 2017, 9, 27135-27141.	8.0	52
68	Construction of Zn2GeO4/Graphene Nanostructures with Dually-Protected Functional Nanoframes for Enhanced Lithium-Storage Performances. Electrochimica Acta, 2017, 251, 129-136.	5.2	18
69	Effect of Fe/Ta doping on structural, dielectric, and electrical properties of Bi ₄ Ti _{2.5} Fe _{0.25} Ta _{0.25} O ₁₂ ceramics. Journal of the American Ceramic Society, 2017, 100, 602-611.	3.8	14
70	Investigation on the Explosive Welding of 1100 Aluminum Alloy and AZ31 Magnesium Alloy. Journal of Materials Engineering and Performance, 2016, 25, 2635-2641.	2.5	42
71	An Insight into the Convenience and Efficiency of the Freeze-Drying Route to Construct 3D Graphene-Based Hybrids for Lithium-Ion Batteries. Electrochimica Acta, 2016, 221, 124-132.	5.2	32
72	Comprehensive investigation of Er2O3 doped (Li,K,Na)NbO3 ceramics rendering potential application in novel multifunctional devices. Journal of Alloys and Compounds, 2016, 683, 171-177.	5.5	37

#	Article	IF	CITATIONS
73	Effect of phase structure changes on the lead-free Er3+-doped (K0.52Na0.48)1â^'Li NbO3 piezoelectric ceramics. Journal of Alloys and Compounds, 2016, 680, 467-472.	5.5	16
74	Effect of reduction/oxidation annealing on the dielectric relaxation and electrical properties of Aurivillius Na _{0.5} Gd _{0.5} Bi ₄ Ti ₄ O ₁₅ ceramics. RSC Advances, 2016, 6, 35102-35109.	3.6	21
75	Low-Molecular-Weight Organo- and Hydrogelators Based on Cyclo(<scp>l</scp> -Lys- <scp>l</scp> -Glu). Langmuir, 2016, 32, 4586-4594.	3.5	44
76	Synthesis of NiO nanostructures and their catalytic activity in the thermal decomposition of ammonium perchlorate. CrystEngComm, 2016, 18, 4836-4843.	2.6	39
77	The role of Fe dopants in phase stability and electric switching properties of Fe-doped VO2. Ceramics International, 2016, 42, 18764-18770.	4.8	34
78	Dimension meditated optic and catalytic performance over vanadium pentoxides. Applied Surface Science, 2016, 389, 112-117.	6.1	20
79	Enhanced Fieldâ€Induced Strain in the Textured Leadâ€Free Ceramic. Journal of the American Ceramic Society, 2016, 99, 3985-3992.	3.8	15
80	Fe2O3 nanocubes exposed (012) active facets combination with graphene rendering enhanced lithium storage capability. Journal of Power Sources, 2016, 327, 658-665.	7.8	56
81	A bubble-template approach for assembling Ni–Co oxide hollow microspheres with an enhanced electrochemical performance as an anode for lithium ion batteries. Physical Chemistry Chemical Physics, 2016, 18, 25879-25886.	2.8	39
82	Effects of Co2+ doping on physicochemical behaviors of hierarchical NiO nanostructure. Applied Surface Science, 2016, 390, 890-896.	6.1	22
83	Hydrothermal growth of VO2 nanoplate thermochromic films on glass with high visible transmittance. Scientific Reports, 2016, 6, 27898.	3.3	32
84	Hydrothermal synthesis and photocatalytic properties of pyrochlore Sm2Zr2O7 nanoparticles. Journal of Photochemistry and Photobiology A: Chemistry, 2016, 321, 48-54.	3.9	29
85	Structural, magnetic and dielectric properties of Bi4Nd0.5Gd0.5Ti3FeO15 ceramics. Ceramics International, 2016, 42, 2806-2812.	4.8	13
86	Effect of Nd ³⁺ substitution for Bi ³⁺ on the dielectric properties and conduction behavior of Aurivillius NdBi ₄ Ti ₃ FeO ₁₅ ceramics. RSC Advances, 2016, 6, 21254-21260.	3.6	17
87	Synthesis and their physicochemical behaviors of flower-like Co3O4 microspheres. Journal of Alloys and Compounds, 2016, 654, 523-528.	5.5	25
88	Improved piezoelectricity and luminescence behavior in Er2O3 doped (K,Na)NbO3 ceramics. Materials Letters, 2016, 162, 226-229.	2.6	24
89	Dielectric relaxations and electrical properties of Aurivillius Bi3.5La0.5Ti2Fe0.5Nb0.5O12 ceramics. Journal of Alloys and Compounds, 2016, 654, 315-320.	5.5	38
90	Grains and grain boundaries contribution to dielectric relaxations and conduction of Bi5Ti3FeO15 ceramics. Journal of Applied Physics, 2015, 118, .	2.5	32

#	Article	IF	CITATIONS
91	Hydrothermal synthesis of cobalt particles with hierarchy structure and physicochemical properties. Materials Research Bulletin, 2015, 72, 7-12.	5.2	13
92	Oxidizing annealing effects on VO2 films with different microstructures. Applied Surface Science, 2015, 345, 232-237.	6.1	59
93	Self-template processed hierarchical V2O5 nanobelts as cathode for high performance lithium ion battery. Electrochimica Acta, 2015, 182, 621-628.	5.2	28
94	Self-Assembling VO ₂ Nanonet with High Switching Performance at Wafer-Scale. Chemistry of Materials, 2015, 27, 7419-7424.	6.7	58
95	Evolution of microstructure in vanadium oxide bolometer film during annealing process. Applied Surface Science, 2015, 357, 887-891.	6.1	13
96	Self-assembly process of China rose-like β-Co(OH) ₂ and its topotactic conversion route to Co ₃ O ₄ with optimizable catalytic performance. CrystEngComm, 2015, 17, 8248-8255.	2.6	22
97	Two-dimensional nanosheets of MoS ₂ : a promising material with high dielectric properties and microwave absorption performance. Nanoscale, 2015, 7, 15734-15740.	5.6	335
98	Contribution of grains and grain boundaries to dielectric relaxations and conduction of Aurivillius Bi4Ti2Fe0.5Nb0.5O12 ceramics. Ceramics International, 2015, 41, 14652-14659.	4.8	24
99	Aggregationâ€Induced Emission Features of Organometal Halide Perovskites and Their Fluorescence Probe Applications. Advanced Optical Materials, 2015, 3, 112-119.	7.3	87
100	Phase separation in Sr doped BiMnO ₃ . Chinese Physics B, 2014, 23, 036401.	1.4	1
101	The enhanced polarization relaxation and excellent high-temperature dielectric properties of N-doped SiC. Applied Physics Letters, 2014, 104, .	3.3	109
102	Enhancing visible-light photoelectrochemical water splitting through transition-metal doped TiO ₂ nanorod arrays. Journal of Materials Chemistry A, 2014, 2, 17820-17827.	10.3	157
103	Dual-band tunable negative refractive index metamaterial with F-Shape structure. Open Physics, 2014, 12, .	1.7	2
104	Spin glass behavior in <i>A</i> -site ordered YBaMn2O6 compound. Journal of Applied Physics, 2013, 114, .	2.5	10
105	Thermodynamic modeling of native defects in ZnO. Optical Materials, 2013, 35, 1213-1217.	3.6	11
106	Design of a novel negative refractive index material based on numerical simulation. EPJ Applied Physics, 2013, 63, 10502.	0.7	4
107	Subsolidus Phase Relations of the <scp><scp>BaO</scp></scp> – <scp>Y</scp> ₂ <scp><scp>O</scp></scp> _{3System in Air. Journal of the American Ceramic Society, 2013, 96, 1332-1336.}	ub≫– <s< td=""><td>cp⊅ <scp>Min</scp></td></s<>	cp⊅ <scp>Min</scp>
108	Structure evolution and entropy change of temperature and magnetic field induced magneto-structural transition in Mn1.1Fe0.9P0.76Ge0.24. Journal of Applied Physics, 2013, 113, .	2.5	11

#	Article	IF	CITATIONS
109	R-site cation randomness effect in theA-site ordered Y0.5La0.5BaMn2O6compound. Chinese Physics B, 2013, 22, 077502.	1.4	1
110	Phase precipitation in the Bi 1â^'x Ca x MnO 3 compounds (x = 0.4–0.6). Europhysics Letters, 2013, 101, 67004.	2.0	0
111	Inhomogeneous Structure and Magnetic Properties of Aurivillius Ceramics <scp><scp>Bi</scp></scp> <scp>TiJournal of the American Ceramic Society, 2013, 96, 3920-3925.</scp>	pૠ&scp≻	<s88>3</s
112	Enhanced photoconductivity of 3C-SiC by Al/N codoping. Journal of Applied Physics, 2013, 114, 104901.	2.5	5
113	The crystal structures and physical properties of the solid solution compound Ba 5 Y 8â^' x Mn 4 O 21â^'1.5 x (x = 0,1). Chinese Physics B, 2012, 21, 066102.	1.4	0
114	Controlled hydrothermal synthesis of tri-wing tellurium nanoribbons and their template reaction. CrystEngComm, 2012, 14, 251-255.	2.6	12
115	Tri-wing bismuth telluride nanoribbons with quasi-periodic rough surfaces. Journal of Materials Chemistry, 2011, 21, 12375.	6.7	15
116	Controlled Synthesis of Tellurium Nanostructures from Nanotubes to Nanorods and Nanowires and Their Template Applications. Journal of Physical Chemistry C, 2011, 115, 6375-6380.	3.1	83
117	Subsolidus phase relations of the Dy-Fe-Al system. Powder Diffraction, 2011, 26, 9-15.	0.2	0
118	Thermodynamics and structural relaxation in Ce-based bulk metallic glass-forming liquids. Journal of Alloys and Compounds, 2011, 509, 4569-4573.	5.5	22
119	A comparative study on characteristic relaxation in Ce65Al10Cu20Co5 and Zr46.75Ti8.25Cu7.5Ni10Be27.5 bulk metallic glasses and supercooled liquids. Intermetallics, 2011, 19, 81-85.	3.9	1
120	Magnetic structure and preferential occupation of Fe in the composite compound Nd2Co6Fe. Physica B: Condensed Matter, 2011, 406, 1995-1999.	2.7	0
121	Neutron diffraction study on composite compound Nd ₂ Co ₇ . Chinese Physics B, 2011, 20, 106101.	1.4	2
122	Phase relations in the ZnO-V ₂ O ₅ -K ₂ O system. Chinese Physics B, 2011, 20, 076402.	1.4	5
123	Structural evolution and physical properties of Bilâ^'xGdxFeO3 ceramics. Acta Materialia, 2010, 58, 3701-3708.	7.9	74
124	Anomalous phase composition in the two-phase region of DyFe _{3â^'<i>x</i>} Al _{<i>x</i>} (<i>x</i> â‰≇.0). Powder Diffraction, 2010, 25, 349-354.	0.2	9
125	Structure, dielectric and magnetodielectric properties of Bi _{1— <i>x</i>} Gd _{<i>x</i>} FeO ₃ Ceramics. Chinese Physics B, 2010, 19, 107505.	1.4	13
126	Synthesis and crystal structure of a novel hexaborate, Na ₂ ZnB ₆ O ₁₁ . Powder Diffraction, 2010, 25, 9-14.	0.2	2

#	Article	IF	CITATIONS
127	The heat capacity measurements of CoSb ₃ -based Skutterudite compounds. International Journal of Materials Research, 2010, 101, 808-811.	0.3	2
128	Tuning Magnetic Properties of α-MnO ₂ Nanotubes by K ⁺ Doping. Journal of Physical Chemistry C, 2010, 114, 8782-8786.	3.1	64
129	Magnetic properties and magnetocaloric effect of Nd(Mn1â^'xFex)2Ge2 compounds. Journal of Alloys and Compounds, 2010, 489, 13-19.	5.5	20
130	Effects of Fe substitution on structural and magnetic properties of the Nd2Co7â^'xFex compounds. Journal of Alloys and Compounds, 2010, 506, 766-771.	5.5	9
131	Ferroelectric transition of Aurivillius compounds Bi5Ti3FeO15 and Bi6Ti3Fe2O18. Applied Physics Letters, 2010, 96, .	3.3	127
132	Spin-glasslike behavior of K+-containing α-MnO2 nanotubes. Journal of Applied Physics, 2009, 105, .	2.5	34
133	Crystal structure determination of K2Zn(PO3)4. Powder Diffraction, 2009, 24, 4-7.	0.2	1
134	Phase composition of arc-melted alloys in the ternary systemCe–Al–Cu (Cu-poor portion). Intermetallics, 2009, 17, 775-779.	3.9	7
135	Magnetic properties and magnetocaloric effect of GdGa compound. Journal of Alloys and Compounds, 2009, 469, 15-19.	5.5	36
136	Phase relations and flux research for zinc oxide crystal growth in the ZnO–K2O–P2O5 system. Journal of Alloys and Compounds, 2009, 470, 336-339.	5.5	4
137	Subsolidus phase relations of the ZnO–Li2O–P2O5 system. Journal of Alloys and Compounds, 2009, 486, 352-356.	5.5	10
138	Synthesis and magnetic properties of antiferromagnetic Co3O4 nanoparticles. Physica B: Condensed Matter, 2008, 403, 3141-3145.	2.7	62
139	Phase diagram of the Bi2O3–Cr2O3 system. Materials Chemistry and Physics, 2008, 112, 239-243.	4.0	21
140	Synthesis of Single-Crystal Tetragonal α-MnO ₂ Nanotubes. Journal of Physical Chemistry C, 2008, 112, 12594-12598.	3.1	244
141	Enhanced ionic conductivity of AgI nanowires/AAO composites fabricated by a simple approach. Nanotechnology, 2008, 19, 495706.	2.6	18
142	Birnessite-type MnO ₂ Nanowalls and Their Magnetic Properties. Journal of Physical Chemistry C, 2008, 112, 17089-17094.	3.1	153
143	Phase relations and flux research for ZnO crystal growth in the ZnO–B2O3–P2O5 system. Journal of Alloys and Compounds, 2008, 459, 481-486.	5.5	10
144	X-ray diffraction analysis and specific heat capacity of (Bi1â^'xLax)FeO3 perovskites. Journal of Alloys and Compounds, 2008, 459, 66-70.	5.5	63

#	Article	IF	CITATIONS
145	Phase relations and flux research for zinc oxide crystal growth in the ZnO–Na2O–P2O5 system. Journal of Alloys and Compounds, 2008, 465, 436-441.	5.5	8
146	A thermodynamic assessment of the copper–gallium system. Calphad: Computer Coupling of Phase Diagrams and Thermochemistry, 2008, 32, 447-453.	1.6	45
147	Experimental study of the phase equilibria of the Ni – Zr system. International Journal of Materials Research, 2008, 99, 712-715.	0.3	5
148	Crystal structure and thermal properties of compound K ₂ Zn ₃ (P ₂ O ₇) ₂ . Powder Diffraction, 2008, 23, 317-322.	0.2	2
149	Phase relations of the Ag–Ga–N system. Journal of Alloys and Compounds, 2007, 429, 184-191.	5.5	12
150	Subsolidus phase relations of the Cu–Ga–N system. Journal of Alloys and Compounds, 2007, 438, 158-164.	5.5	14
151	A new structure type of phosphate: Crystal structure of Na2Zn5(PO4)4. Journal of Solid State Chemistry, 2007, 180, 2256-2261.	2.9	17
152	Magnetic properties of Bi(Fe1â^xCrx)O3 synthesized by a combustion method. Applied Physics Letters, 2007, 90, 162513.	3.3	68
153	Thermodynamic assessment of the Ag–Ga system. Calphad: Computer Coupling of Phase Diagrams and Thermochemistry, 2006, 30, 316-322.	1.6	20
154	Thermodynamic analysis of Mg-doped p-type GaN semiconductor. Journal of Alloys and Compounds, 2006, 422, 279-282.	5.5	5
155	Structural transition in unpoled (1â^x)PMN–xPT ceramics near the morphotropic boundary. Journal of Alloys and Compounds, 2006, 425, 373-378.	5.5	26
156	Design of shallow acceptors inZnO: First-principles band-structure calculations. Physical Review B, 2006, 74, .	3.2	198
157	Structures of the ζ and ζ′ phases in the Ag–Ga system. Journal of Alloys and Compounds, 2005, 399, 155-159.	5.5	20
158	Effect of Ti on the Stability of Phases in the (1 â^' x)Pb(Mg1/3Nb2/3)O3-xPbTiO3Solid Solution. Ferroelectrics, 2004, 313, 71-80.	0.6	9
159	Thermodynamic Analysis of the Ga—Ti System ChemInform, 2003, 34, no.	0.0	0
160	Thermodynamic analysis of the Ga–Ti system. Journal of Alloys and Compounds, 2003, 358, 133-141.	5.5	12
161	Development of thermodynamic modeling of oxygen-doped GaN semiconductor. Calphad: Computer Coupling of Phase Diagrams and Thermochemistry, 2003, 27, 1-8.	1.6	3
162	A Thermodynamic Assessment of the In–Se System. International Journal of Materials Research, 2003, 94, 381-389.	0.8	12

#	Article	IF	CITATIONS
163	Thermodynamic modeling of native point defects and dopants of GaN semiconductors. Journal of Electronic Materials, 2002, 31, 321-326.	2.2	19
164	Computer simulations of phase transformation in steels. Materials & Design, 2001, 22, 39-43.	5.1	7
165	A thermodynamic reassessment of the Al-As-Ga system. Journal of Phase Equilibria and Diffusion, 2001, 22, 26-33.	0.3	11
166	A thermodynamic assessment of the Ga-In-P system. Journal of Phase Equilibria and Diffusion, 2000, 21, 357-363.	0.3	12
167	Thermodynamic analysis of the Ga–In–As–Sb–C–H system. Journal of Crystal Growth, 1999, 207, 20-20	6.1.5	0
168	Assessment of phase diagram and thermodynamic properties of the Al-Ga-Sb system. Journal of Phase Equilibria and Diffusion, 1999, 20, 316-323.	0.3	7
169	A thermodynamic assessment of the Ga-As-Sb system. Journal of Phase Equilibria and Diffusion, 1998, 19, 466-472.	0.3	12
170	A thermodynamic assessment of the In-As-Sb system. Journal of Phase Equilibria and Diffusion, 1998, 19, 473-478.	0.3	8